Cell-centered Lagrangian scheme for multi-material flows with pressure equilibration

B. Manach-Perennou[1], R. Chauvin, S. Guisset, A. Llor

Abstract. A cell-centered Lagrangian scheme is presented for the multimaterial hydrodynamics model with equal pressure assumption. The scheme is conservative in mass, momentum and total energy while being entropic per material. This last point is critical for various engineer applications but remains in general not addressed. The entropy dissipation of each material is taken as an arbitrary portion of the global entropy dissipation hence mimicking different viscosity operators and the underlying vanishing viscosity solution. The scheme is confronted with different 1 or 2-dimensional test cases where materials have highly different equations of state. These test cases attest the robustness of the scheme and show that pressures are kept equal up to the scheme order or even strictly if an additional relaxation procedure is added.

Key words. Cell-centered Lagrangian scheme, multi-material flows, entropy dissipation.

[1]CEA-DIF, France. E-mail: bastien.manach-perennou@cea.fr

Contents

1 Introduction

In the context of multimaterial flows, interface widths between materials are significantly smaller than observation scales for many applications and may then be considered as sharp discontinuities. The modeling and numerical treatment of these interfaces may be done in numerous ways which accounts for the multiplicity of methods developed over the past few decades. Among all available methods, two categories have emerged in order to handle multiphases interface. The first one which does not allow any phase mixing is often referred as sharp interface methods [21, 11] while the second one deals with interfaces as a diffuse area in which the interface is not clearly defined. In the first category falls standard front tracking and Lagrangian methods [29, 1] for which the mesh is adapted (or naturally adapts) to follow the interface. In this group, one may also find several methods based on reconstruction techniques [22]. Here we also mention other very popular numerical strategy [13, 10, 28]. Concerning the second category, while early ideas have been introduced in [3], diffuse interface methods have been gaining popularity lately [27, 19]. They consist in deliberately allowing the interface to spread over a controlled width thus bypassing potential geometric difficulties which are the main drawback of sharp interface methods. They also allow the easy integration of additional physical phenomena such as capillarity, surface tension, drag forces and added mass among others [12]. The inherent numerical smearing of the interfaces results in a certain loss of accuracy that still may be mitigated by anti-diffusive methods [23]. A detailed review of diffuse interface models and schemes may be found in [27, 19].

Multiple models may be considered when dealing with multimaterial flows in the framework of diffuse interface method. The one under consideration in this article is obtained through a conditional averaging procedure introduced in [14] and extensively described in [32, 17]. More precisely, single material Euler equations with discontinuous thermodynamic properties are initially considered, together with proper boundary conditions at interfaces and borders of the domain. These equations are duplicated by multiplying them with mass fractions, thus obtaining a set of equations per material (in our case, momentum equations are redundant as materials are assumed to have the same velocity). The resulting augmented system then undergoes an averaging procedure. Finally, some terms still need to be specified with physical assumptions.

In the present article, we focus on two closures for the volume fractions evolution: the equal-strain and equal-pressure assumptions. The former consists in assuming volume fractions stay constant during the Lagrangian phase; in other words, all materials are compressed or expanded with the same rate. It is quite convenient and widely used in numerical simulations of multimaterial flows [2]. However, it leads to a strong pressure decoupling inside of material mixtures with significantly different equations of state (e.g. mixtures of air and water). For these reasons, another closure is necessary for some applications and the equal pressure assumption is a sound one [15]. With this closure, pressures are kept equal at all times. Enforcing pressure equality may be done at the discrete level by solving a non-linear system of equation [9] through an

iterative method. This article follows the ideas developed in [31] by computing the evolution equation for the volume fraction and then discretizing it. As a result, the scheme is fully explicit and does not rely on any iterative solver. Modifier avec les modifs de Remi ??

Our scheme is based on a cell-centered Lagrange-remap procedure, the remapping procedure being standard and only used if necessary for 2D test cases with strong mesh entanglement. The Lagrangian part, which constitutes the main contribution of this article, is an extension of the Eucclhyd scheme [4, 24], written in internal energy [7, 6], to multimaterial flows. It needs to be highlighted that the internal energy formulation is uncommon for cell-centered schemes but is essential here. Firstly, it allows for an accurate control of each species entropy dissipation. More precisely, the semi-continuous scheme is constructed so that entropy variation is positive for each material, thus ensuring thermodynamic consistency of our approach. While being critical for various engineer applications this point is very often not addressed and, in our opinion, makes this work valuable to the community. Secondly, the species internal energy formulation is convenient for the numerical strategy presented here and enables to enforce pressures equality up to the scheme order. The resulting scheme is exactly conservative in mass, momentum and total energy (i.e. the sum of kinetic energy and all material internal energies) at the discrete level.

Not only entropy dissipation is positive for each material, but ratios between materials may be freely customized. It is a key feature of the scheme and our answer to the presence of non-conservative terms in the model, following the work made in [8]. Contrary to hyperbolic conservation laws, non-conservative systems of equation do not admit a canonical solution. Solutions may then be defined with an added vanishing regularization operator or with a choice of path [20] which defines generalized Rankine-Hugoniot jump conditions. The latter choice inspired the methodology described in [5] for a path-dependent scheme based on in-cell reconstruction techniques and exact resolution of Riemann problems. Our approach, based on [8], is related to vanishing regularization operators which are mimicked at the discrete level by a choice of entropy dissipation distribution. Still, it is a decent answer to the issue of thermodynamic consistency and the multiplicity of solutions arising from the presence of non-conservative terms.

The article is organized as follows. In section 2, the two different closures (namely equal-strain and equal-pressure) for multimaterial models are presented. The numerical scheme is then detailed in section 3, together with a note on the pressure relaxation procedure found in [9, 12]. Finally, the scheme is confronted with 1D and 2D test cases (some of which displaying highly contrasted equation of states) and results are compared between both equal strain and equal pressure closures.

2 Closures for multi-material models

In this section two multi-material models are presented. The first one considers the equal strain assumption which is commonly used for the simulation of multi-material flows. However, it may become particularly irrelevant in the case of materials with strongly different compressibilities. The second one considers variable volume fractions which always remains valid but requires a more challenging numerical treatment.

2.1 Notations

Let n be the number of material. In the present document the mass fraction of material k is denoted c^k, its volume fraction by α^k and its density by ρ^k. Inside a given volume V where a mass m^k of material k occupies a volume V^k, these quantities are defined as follows

$$c^k = \frac{m^k}{m}, \qquad \alpha^k = \frac{V^k}{V}, \qquad \rho^k = \frac{m^k}{V^k}.$$

The total density of the mixture may also be defined as

$$\rho = \frac{m}{V} = \sum_k \alpha^k \rho^k.$$

Additionally, internal energy of material k is denoted e^k and its pressure p^k. The quantities ρ^k, e^k and p^k are related to each other with an equation of state $p^k(\rho^k, e^k)$. The total pressure of the mixture is then chosen to be

$$p = \sum_k \alpha^k p^k = \sum_k \alpha^k p^k(\rho^k, e^k).$$

Finally, the characteristic times at which material velocities relax to a common value is assumed to be significantly smaller than the characteristic times of observation so that only one common velocity $\mathbf{u}$ is considered.

2.2 Multi-material model with equal strain assumption

A first model, already widely documented [2] , is now presented. The dynamic of the different materials is described by their density ρ^k, volume fraction α^k, velocity $\mathbf{u}$ and internal energy e^k. The conservation equations written in semi-updated Lagrangian formalism reads

$$\begin{cases} \rho^k \dfrac{\mathrm{d}}{\mathrm{d}t}\left(\dfrac{1}{\rho^k}\right) - \nabla \cdot \mathbf{u} = 0, \\ \rho \dfrac{\mathrm{d}}{\mathrm{d}t}\left(\mathbf{u}\right) + \nabla p = 0, \\ \rho^k \dfrac{d}{dt}\left(e^k\right) + p^k \nabla \cdot \mathbf{u} = 0, \end{cases} \tag{1}$$

At this point the set of equations (1) must be completed with an additional closure relation since no information is given concerning the evolution of volume fractions α^k. The equal strain assumption is traditionally introduced to describe the temporal evolution of the volume fractions

$$\frac{\mathrm{d}}{\mathrm{d}t}(\alpha^k) = 0, \quad \forall k \in \{1, ..., n\}. \tag{2}$$

This resulting model is largely used for the simulation of multi-material flows, since is does not imply strong modifications of the practical algorithm starting from a mono-material code. The numerical treatment of the set of equation is standard and for clarity we do not intend to detail it here. Instead we refer to [2] in which this is clearly explained.

2.3 Multi-material model with no equal strain assumption

In order to handle strongly different material deformation rates (as for water and air mixtures) the following model is introduced

$$\begin{cases} \alpha^k \rho^k \dfrac{\mathrm{d}}{\mathrm{d}t}\left(\dfrac{1}{\alpha^k \rho^k}\right) - \nabla \cdot \mathbf{u} = 0, \\ \rho \dfrac{\mathrm{d}}{\mathrm{d}t}(\mathbf{u}) + \nabla p = 0, \\ \alpha^k \rho^k \dfrac{\mathrm{d}}{\mathrm{d}t}(e^k) = -\alpha^k \rho^k p^k \dfrac{\mathrm{d}}{\mathrm{d}t}\left(\dfrac{1}{\rho^k}\right). \end{cases} \tag{3}$$

This model is obtained through a conditional averaging procedure introduced in [14] and extensively described in [32, 17]. Once again the system is underdetermined and must be supplemented with a closure relationship on the volume fractions (or equivalently, on the densities). Under the equal strain assumption (2), both models (1) and (3) may be shown to be equivalent so that the latter is somewhat a generalization of the former, hence paving the way for other closures. Notice however that the conservation of the total energy is not ensured for an arbitrary total pressure p. It is formally ensured if the total pressure is defined as

$$p = \sum_k \theta^k p^k, \qquad \theta^k = \frac{\alpha^k \rho^k \dfrac{\mathrm{d}}{\mathrm{d}t}\left(\dfrac{1}{\rho^k}\right)}{\displaystyle\sum_l \alpha^l \rho^l \frac{\mathrm{d}}{\mathrm{d}t}\left(\frac{1}{\rho^l}\right)},$$

which gives back the formula $p = \sum_k \alpha^k p^k$ in the context of equal strain assumption.

2.4 Isobar assumption: from implicit to explicit formulation

In all multi-material flows applications we are interested in, the pressure relaxation process between materials occurs on time scale much smaller compared to

the hydrodynamics characteristics time scales [15]. Consequently, the equality between all material pressures is considered. This is also known as the isobar assumption or single pressure constraint

$$p = p^k(\rho^k, e^k), \quad \forall k \in \{1, ..., n\}, \tag{4}$$

which provides an implicit closure on the volume fractions and densities. Following [30], in order to make use of equations (4), we explicitly derive the underlying rates of expansion $\frac{\mathrm{d}}{\mathrm{d}t}(\rho^k)$. The conservation of the total mass gives a relationship between all terms $d_t\rho^k$

$$\sum_k \left[\rho^k \alpha^k \frac{\mathrm{d}}{\mathrm{d}t}\left(\frac{1}{\alpha^k \rho^k}\right) - \nabla \cdot u\right] \alpha^k = 0, \tag{5}$$

$$\iff \sum_k \left[\frac{\alpha^k}{\rho^k}\frac{\mathrm{d}}{\mathrm{d}t}(\rho^k) + \frac{\mathrm{d}}{\mathrm{d}t}(\alpha^k)\right] = -\nabla \cdot u, \tag{6}$$

$$\iff \sum_k \frac{\alpha^k}{\rho^k}\frac{\mathrm{d}}{\mathrm{d}t}(\rho^k) = -\nabla \cdot u. \tag{7}$$

On the other hand, differentiating (4) with respect to time (both Eulerian and Lagrangian time derivatives are equivalent because materials all share the same velocity) and making use of thermodynamic considerations lead to

$$\frac{\mathrm{d}}{\mathrm{d}t}(p) = \frac{\mathrm{d}}{\mathrm{d}t}(p^k) = (c^k)^2 \frac{\mathrm{d}}{\mathrm{d}t}(\rho^k) + \rho^k \Gamma^k T^k \frac{\mathrm{d}}{\mathrm{d}t}(\eta^k). \tag{8}$$

Finding $\frac{\mathrm{d}}{\mathrm{d}t}(\rho^k)$ essentially amounts to solving the linear system formed by the $N+1$ previous equation with unknowns $\{\frac{\mathrm{d}}{\mathrm{d}t}(p), \left(\frac{\mathrm{d}}{\mathrm{d}t}(\rho^k)\right)_k\}$. Substituting $\frac{\mathrm{d}}{\mathrm{d}t}(\rho^k)$ with $\frac{1}{(c^k)^2}(\frac{\mathrm{d}}{\mathrm{d}t}(p) - \rho^k \Gamma^k T^k \frac{\mathrm{d}}{\mathrm{d}t}(\eta^k))$ inside equation (7) gives

$$\frac{\mathrm{d}}{\mathrm{d}t}(p) = -\frac{1}{\sum_k \frac{\alpha_k}{\rho^k (c^k)^2}} \nabla \cdot u + \sum_k \beta^k \rho^k \Gamma^k T^k \frac{\mathrm{d}}{\mathrm{d}t}(\eta^k),$$
$$\beta^k = \frac{\frac{\alpha^k}{\rho^k (c^k)^2}}{\sum_l \frac{\alpha^l}{\rho^l (c^l)^2}}.$$

Notice that $\sum_k \beta^k = 1$. At this point, the unknowns $\frac{\mathrm{d}}{\mathrm{d}t}(\rho^k)$ are immediately recovered:

$$\begin{aligned} \alpha^k \rho^k \frac{\mathrm{d}}{\mathrm{d}t}\left(\frac{1}{\rho^k}\right) &= \beta^k \nabla \cdot u + \left(\sum_l \frac{\alpha^l}{\rho^l (c^l)^2}\right) \sum_l \beta^k \beta^l \Delta^{kl}, \\ \Delta^{kl} &= \rho^k \Gamma^k T^k \frac{\mathrm{d}}{\mathrm{d}t}(\eta^k) - \rho^l \Gamma^l T^l \frac{\mathrm{d}}{\mathrm{d}t}(\eta^l). \end{aligned} \tag{9}$$

In the case of model (3), which is isentropic, one has

$$\begin{cases} \alpha^k \rho^k \dfrac{\mathrm{d}}{\mathrm{d}t}\left(\dfrac{1}{\rho^k}\right) - \beta^k \nabla \cdot \mathbf{u} = 0, \\ \alpha^k \rho^k \dfrac{\mathrm{d}}{\mathrm{d}t}\left(e^k\right) + p^k \beta^k \nabla \cdot \mathbf{u} = 0, \end{cases} \tag{10}$$

which is equivalent to the equal strain hypothesis if we replace β^k with α^k. This essentially means that inside a given volume containing multiple materials, the expansion of the total volume is no longer shared between materials with respect to their volume fractions α^k. It is instead shared with respect to the coefficient β^k, which takes into account thermodynamic properties of the different materials.

Remark: Regarding the previous considerations on total energy conservation, one automatically recovers it from the equality of pressures. This property will need to be ensured at the discrete level with the chosen numerical strategy.

3 Numerical strategy

The numerical strategy used for the discretization of system (3)-(4) is now presented. The strategy is based on the continuous equations (9) derived in the previous section. This allows us not to rely on an iterative procedure to deal with the strongly non-linear and potentially stiff implicit initial formulation of the model (4). The resulting scheme is then fully explicit, conserves mass, momentum and total energy while ensuring a positive entropy dissipation for each material.

3.1 Geometry and notations

The notations used are similar to the ones introduced in [18, 6]. Each cell is assigned a unique index c and is denoted ω_c. Its volume is V_c. The cells are assumed to be polygonal so that they are defined by the set of their nodes $\mathcal{P}(c)$. The neighbor cells are collected in the set $\mathcal{N}(c)$. For a given node p, $\mathcal{C}(p)$ is the set of cells that contains p. We write x_p and u_p for its position and velocity. We denote p^+ the node in $\mathcal{P}(c)$ which follows p in counterclockwise order and p^- the previous node. Let $\mathbf{n}_{pc}^+$ be the outward normal unit vector to $\vec{pp^+}$ and consider $l_{pc}^+ = \frac{1}{2}\left\|\vec{pp^+}\right\|$. Similarly, $\mathbf{n}_{pc}^-$ and l_{pc}^- are defined accordingly. Consequently, the corner outward normal unit vector $\mathbf{n}_{pc}$ is defined as follows

$$\mathbf{n}_{pc} = \frac{l_{pc}^+ \mathbf{n}_{pc}^+ + l_{pc}^- \mathbf{n}_{pc}^-}{l_{pc}}, \qquad l_{pc} = \left\| l_{pc}^+ \mathbf{n}_{pc}^+ + l_{pc}^- \mathbf{n}_{pc}^- \right\|_2 .$$

Finally, V_{pc} denotes the volume formed by p, $\|\vec{pp^+}\|/2$, x_c and $\|\vec{pp^-}\|/2$. The quantity V_p is the volume around p defined by

$$V_p = \sum_{p \in \mathcal{P}(c)} V_{pc}.$$

All the notations introduced are illustrated in Figure 1.

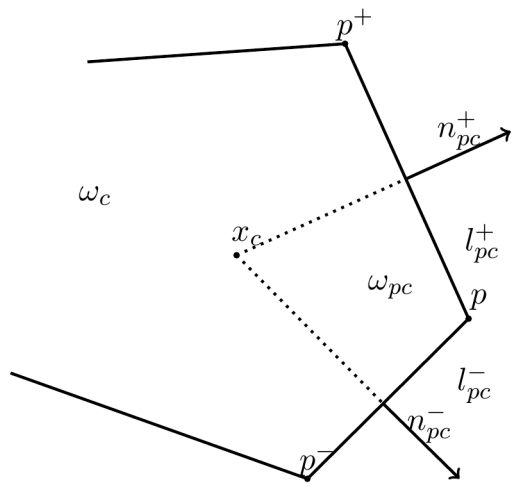

Figure 1: Cell notations.

3.2 Total volume and momentum conservation equations

Regarding the mass and momentum equations discretization, no significant changes are made from the classical EUCCLHYD scheme [18]. The numerical strategy is briefly recalled here, along with the definition of cell variables. The approach is that of a finite volume scheme. Consequently, for physical quantities $\phi \in \left\{ \frac{1}{\alpha^k \rho^k}, e^k, \frac{1}{\rho^k} \right\}$ related to material k and a cell c, are defined the averaged quantities over the cell by:

$$m_c^k = \int_{\omega_c} \alpha^k \rho^k \mathrm{d}\mathbf{x}, \qquad \phi_c = \frac{1}{m_c^k} \int_{\omega_c} \alpha^k \rho^k \phi \mathrm{d}\mathbf{x},$$

$$m_c = \int_{\omega_c} \rho \mathrm{d}\mathbf{x}, \qquad \mathbf{u}_c = \frac{1}{m_c} \int_{\omega_c} \rho \mathbf{u} \mathrm{d}\mathbf{x}.$$

Remark: In the following, ρ_c^k denotes the inverse of $\left(1/\rho^k\right)_c$ which is technically different from the weighted average value of ρ^k over the cell. Same goes for the notation $(\alpha^k \rho^k)_c$. Finally α_c^k is defined as the division of $(\alpha^k \rho^k)_c$ by ρ^k so that $(\alpha^k \rho^k)_c = \alpha_c^k \rho_c^k$ (this type of equality is generally not trivial when working with averaged values). With this definition, the α_c^k satisfy

$$\sum_k \alpha^k = \sum_k \frac{\left(\dfrac{1}{\rho^k}\right)_c}{\left(\dfrac{1}{\alpha^k \rho^k}\right)_c} = \sum_k \frac{\displaystyle\int_{\omega_c} \alpha^k \mathrm{d}\mathbf{x}}{\displaystyle\int_{\omega_c} 1 \mathrm{d}\mathbf{x}} = 1.$$

Defining these averaged quantities prepares for the use of Reynold's transport theorem which implies that

$$\frac{\mathrm{d}}{\mathrm{d}t}\int_{\omega_c}\alpha^k\rho^k\phi\mathrm{d}\mathbf{x} = m_c^k\frac{\mathrm{d}}{\mathrm{d}t}\phi_c, \quad \phi\in\left\{\frac{1}{\alpha^k\rho^k}, e^k, \frac{1}{\rho^k}\right\},$$

$$\frac{\mathrm{d}}{\mathrm{d}t}\int_{\omega_c}\rho\mathbf{u}\mathrm{d}\mathbf{x} = m_c\frac{\mathrm{d}}{\mathrm{d}t}\mathbf{u}_c.$$

The mass conservation equation, averaged over a Lagrangian cell, then gives:

$$m_c^k\frac{\mathrm{d}}{\mathrm{d}t}\left(\frac{1}{\alpha_c^k\rho_c^k}\right) = \oint_{\partial\omega_c}\mathbf{u}\cdot\mathbf{n}\mathrm{d}l = \sum_{p\in\mathcal{P}(c)} l_{pc}\mathbf{n}_{pc}\cdot\mathbf{u}_p. \tag{11}$$

The left hand-side may be interpreted as a sum of node fluxes. Considering that the cell remains polygonal through advection, its volume only depends on nodes position. Then, equation (11) may also be seen as the exact derivative of the Lagrangian volume, using the chain rule and the formula $\frac{\partial V_c}{\partial\mathbf{x}_p} = l_{pc}\mathbf{n}_{pc}$. More detail may be found in [18]. In order to proceed with the analysis of the momentum conservation equation, we define sub-cell forces as follows

$$\mathbf{f}_{pc} = -\int_{\partial\omega_{pc}\cap\partial\omega_c} p\mathbf{n}\mathrm{d}l.$$

For the momentum conservation, Green's formula simply leads to

$$m_c\frac{\mathrm{d}\mathbf{u}_c}{\mathrm{d}t} = -\int_{\omega_c}\nabla p\mathrm{d}\mathbf{x} = -\int_{\partial\omega_c} p\mathbf{n}\mathrm{d}l = \sum_{p\in\mathcal{P}(c)} -\int_{\partial\omega_{pc}\cap\partial\omega_c} p\mathbf{n}\mathrm{d}l = \sum_{p\in\mathcal{P}(c)}\mathbf{f}_{pc}. \tag{12}$$

In the spirit of [18] the closure procedure to compute $\mathbf{f}_{pc}$ is chosen to guarantee a correct species dissipation entropy as well as to ensure the momentum and total energy conservation. These properties will be proven in the discrete property section

$$\mathbf{f}_{pc} = -l_{pc}p_c\mathbf{n}_{pc} + (\mathbf{u}_p - \mathbf{u}_c)^T\mathbf{M}_{pc}, \tag{13}$$

where $\mathbf{M}_{pc}$ is a semi-positive defined matrix called in the following a dissipation matrix. Now, in order to enforce a correct discrete species entropy dissipation, the following standard dissipation matrix definition [24] is taken

$$\mathbf{M}_{pc} = \rho_c c_c^s\left(l_{pc}^+\mathbf{n}_{pc}^+\otimes\mathbf{n}_{pc}^+ + l_{pc}^-\mathbf{n}_{pc}^-\otimes\mathbf{n}_{pc}^-\right), \tag{14}$$

where c_c^s is the speed of sound.

3.3 Species internal energy and density equations

A naive discretization of the energy and density equations would consist in

$$\left\{\begin{aligned} m_c^k \frac{\mathrm{d}}{\mathrm{d}t}(e_c^k) &= -p_c m_c^k \frac{\mathrm{d}}{\mathrm{d}t}\left(\frac{1}{\rho^k}\right), \\ m_c^k \frac{\mathrm{d}}{\mathrm{d}t}\left(\frac{1}{\rho^k}\right) &= -\beta_c^k \sum_{p\in\mathcal{P}(c)} l_{pc}\mathbf{n}_{pc}\cdot\mathbf{u}_p. \end{aligned}\right. \tag{15}$$

However, when comparing the suggested discretization (15) with the standard mono-material scheme, one understands that some numerical dissipation needs to be added in order to stabilize the scheme. This numerical dissipation physically translates into entropy dissipation so that we consider the non-isentropic equations (i.e. the fundamental thermodynamics relation and equation (9) for each material k)

$$\left\{\begin{aligned} m_c^k \frac{\mathrm{d}}{\mathrm{d}t}\left(e_c^k\right) &= -p\, m_c^k \frac{\mathrm{d}}{\mathrm{d}t}\left(\frac{1}{\rho_c^k}\right) + \int_{\omega_c} \alpha^k\rho^k T^k d_t(\eta^k), \\ m_c^k \frac{\mathrm{d}}{\mathrm{d}t}\left(\frac{1}{\rho_c^k}\right) &= -\beta_c^k \sum_{p\in\mathcal{P}(c)} l_{pc}\mathbf{n}_{pc}\cdot\mathbf{u}_p + \int_{\omega_c}\left(\sum_l \frac{\alpha^l}{\rho^l (c^l)^2}\right)\sum_l \beta^k\beta^l\Delta^{kl}. \end{aligned}\right.$$

The discretization of the term $\alpha^k\rho^k T^k d_t(\eta^k)$ (also appearing inside the expression of Δ^{lk}) needs to be specified to enforce the chosen numerical viscosity per species. We first consider the conservation of the total energy $\sum_k \alpha^k\rho^k e^k$ whose equation should be discretized according to the monomaterial scheme

$$\sum_k m_c^k \frac{\mathrm{d}}{\mathrm{d}t}(e_c^k) = \sum_{p\in\mathcal{P}(c)} \mathbf{f}_{pc}\cdot(\mathbf{u}_p - \mathbf{u}_c),$$

which gives

$$\sum_k \int_{\omega_c} \alpha^k\rho^k T^k d_t(\eta^k) = \sum_{p\in\mathcal{P}(c)} (\mathbf{u}_p - \mathbf{u}_c)^T \mathbf{M}_{pc}(\mathbf{u}_p - \mathbf{u}_c).$$

The total entropy dissipation now needs to be shared between materials through coefficients $\lambda^k > 0$ such that $\sum_k \lambda^k = 1$. The species discrete numerical viscosity is then written

$$\begin{aligned} \int_{\omega_c} \alpha^k\rho^k T^s d_t(\eta^k) &= \lambda^k \left[\sum_{p\in\mathcal{P}(c)} (\mathbf{u}_p - \mathbf{u}_c)^T \mathbf{M}_{pc}(\mathbf{u}_p - \mathbf{u}_c)\right], \\ &= \sum_{p\in\mathcal{P}(c)} (\mathbf{u}_p - \mathbf{u}_c)^T \mathbf{M}_{pc}^k(\mathbf{u}_p - \mathbf{u}_c), \qquad \left(\mathbf{M}_{pc}^k = \lambda^k \mathbf{M}_{pc}\right). \end{aligned}$$

The choice of the coefficients λ^k is no simple matter and does more than only stabilizing the scheme. Indeed, it is well-known [20, 5] that non-conservative hyperbolic systems, such as the one under study here, have no canonical solution as vanishing viscosity solutions depend on the diffusion operator; this is not the case for conservative hyperbolic systems. Hence, different choices of λ^k will produce different numerical solutions [8] and they should be chosen according to physical considerations and the user's expertise. For our test cases, we chose λ^k as the mass fraction of material k. Finally, our space discretization is

$$\left\{\begin{aligned} m_c^k \frac{\mathrm{d}}{\mathrm{d}t}\left(e_c^k\right) &= -p_c\, m_c^k \frac{\mathrm{d}}{\mathrm{d}t}\left(\frac{1}{\rho_c^k}\right) + \sum_{p\in\mathcal{P}(c)} (\mathbf{u}_p - \mathbf{u}_c)^T \mathbf{M}_{pc}^k (\mathbf{u}_p - \mathbf{u}_c), \\ m_c^k \frac{\mathrm{d}}{\mathrm{d}t}\left(\frac{1}{\rho_c^k}\right) &= -\beta_c^k \sum_{p\in\mathcal{P}(c)} l_{pc}\mathbf{n}_{pc}\cdot\mathbf{u}_p + \left(\sum_l \frac{\alpha_c^l}{\rho_c^l (c_c^l)^2}\right) \sum_l \beta_c^k \beta_c^l \Delta_c^{kl}, \\ \Delta_c^{kl} &= \sum_{p\in\mathcal{P}(c)} (\mathbf{u}_p - \mathbf{u}_c)^T \left(\frac{\Gamma_c^k}{\alpha_c^k}\mathbf{M}_{pc}^k - \frac{\Gamma_c^l}{\alpha_c^l}\mathbf{M}_{pc}^l\right)(\mathbf{u}_p - \mathbf{u}_c). \end{aligned}\right.$$

The only thing missing in the semi-discrete scheme is the expression of the node velocities $\mathbf{u}_p$. As in the monomaterial scheme, they are computed as follows

$$\mathbf{u}_p = \left[\sum_{c\in\mathcal{C}(p)} \mathbf{M}_{pc}\right]^{-1} \left(\sum_{c\in\mathcal{C}(p)} (p_c l_{pc}\mathbf{n}_{pc} - \mathbf{M}_{pc}\mathbf{u}_c)\right).$$

This equation is equivalent to $\sum_{c\in\mathcal{C}(p)} \mathbf{f}_{pc} = 0$, which ensures both the momentum and total energy semi-discrete conservation (see next section).

3.4 Time discretization

A standard Euler forward strategy is chosen for the time discretization of the equations. The scheme is then explicit, all spatial terms derived in the previous sections being taken at the initial time. Some caution may still need to be exercised on the velocity $\mathbf{u}_c$ inside the energy equation. Indeed, taking an average value $(\mathbf{u}_c^{n+1} + \mathbf{u}_c^n)/2$ is necessary for the discrete total energy conservation as it will be discussed in the next section. The resulting scheme is still fully explicit as velocities may be computed before energies.

$$
\begin{cases}
\dfrac{m_c^k}{\Delta t}\left(\dfrac{1}{(\alpha\rho)_c^{k,n+1}}-\dfrac{1}{(\alpha\rho)_c^{k,n}}\right)=\displaystyle\sum_{p\in\mathcal{P}(c)} l_{pc}\mathbf{n}_{pc}\cdot\mathbf{u}_p^n,\\[2ex]
m_c\dfrac{\mathbf{u}_c^{n+1}-\mathbf{u}_c^n}{\Delta t}=\displaystyle\sum_{p\in\mathcal{P}(c)}\mathbf{f}_{pc}^n,\\[2ex]
m_c^k\dfrac{e_c^{k,n+1}-e_c^{k,n}}{\Delta t}=-p_c^n\dfrac{m_c^k}{\Delta t}\left(\dfrac{1}{\rho_c^{k,n+1}}-\dfrac{1}{\rho_c^{k,n}}\right)+\displaystyle\sum_{p\in\mathcal{P}(c)}(\mathbf{u}_p^n-\mathbf{u}_c^n)^T\mathbf{M}_{pc}^{k,n}\left(\mathbf{u}_p^n-\dfrac{\mathbf{u}_c^n+\mathbf{u}_c^{n+1}}{2}\right),\\[2ex]
\dfrac{m_c^k}{\Delta t}\left(\dfrac{1}{\rho_c^{k,n+1}}-\dfrac{1}{\rho_c^{k,n}}\right)=-\beta_c^{k,n}\displaystyle\sum_{p\in\mathcal{P}(c)} l_{pc}\mathbf{n}_{pc}\cdot\mathbf{u}_p^n+\left(\sum_l\dfrac{\alpha_c^{l,n}}{\rho_c^{l,n}(c_c^{l,n})^2}\right)\sum_l\beta_c^{k,n}\beta_c^{l,n}\Delta_c^{kl,n},\\[2ex]
\Delta_c^{kl,n}=\displaystyle\sum_{p\in\mathcal{P}(c)}(\mathbf{u}_p^n-\mathbf{u}_c^n)^T\left(\dfrac{\Gamma_c^{k,n}}{\alpha_c^{k,n}}\mathbf{M}_{pc}^{n,k}-\dfrac{\Gamma_c^{l,n}}{\alpha_c^{l,n}}\mathbf{M}_{pc}^{l,n}\right)\left(\mathbf{u}_p^n-\dfrac{\mathbf{u}_c^n+\mathbf{u}_c^{n+1}}{2}\right).
\end{cases}
\tag{16}
$$

In the next section the main numerical properties are presented.

3.5 Numerical properties

In this section the positiveness of the temperatures, discrete total energy conservation and semi-discrete entropy dissipation are proven.

Property 1. *Discrete total energy conservation*
The total discrete energy is conserved

$$
\sum_c m_c\left(e_c^{n+1}+\left\|\boldsymbol{u}_c^{n+1}\right\|^2/2\right)=\sum_c m_c\left(e_c^n+\|\boldsymbol{u}_c^n\|^2/2\right).
$$

Proof. Multiplying equation (12) by $(\mathbf{u}_c^{n+1}+\mathbf{u}_c^n)/2$ one obtains

$$
\frac{m_c}{2\Delta t}\left(\left\|\mathbf{u}_c^{n+1}\right\|^2-\|\mathbf{u}_c^n\|^2\right)=\sum_{p\in\mathcal{P}(c)}\mathbf{f}_{pc}^n\cdot\left(\frac{\mathbf{u}_c^{n+1}+\mathbf{u}_c^n}{2}\right). \tag{17}
$$

On the other hand, adding the N energy equations given in (16) leads to

$$\begin{aligned}
m_c \frac{e_c^{n+1} - e_c^n}{\Delta t} &= \sum_k p_c m_c^k \left(\frac{1}{\rho_c^{k,n+1}} - \frac{1}{\rho_c^{k,n}} \right) + \sum_{p \in \mathcal{P}(c)} (\mathbf{u}_p - \mathbf{u}_c)^{\mathrm{T}} \mathbf{M}_{pc} \left(\mathbf{u}_p - \frac{\mathbf{u}_c^{n+1} + \mathbf{u}_c^n}{2} \right) \\
&= -p_c \sum_{p \in \mathcal{P}(c)} l_{pc} \mathbf{n}_{pc} \cdot \left(\mathbf{u}_p - \frac{\mathbf{u}_c^{n+1} + \mathbf{u}_c^n}{2} \right) + \sum_{p \in \mathcal{P}(c)} \mathbf{M}_{pc} (\mathbf{u}_p - \mathbf{u}_c) \cdot \left(\mathbf{u}_p - \frac{\mathbf{u}_c^{n+1} + \mathbf{u}_c^n}{2} \right) \\
&= \sum_{p \in \mathcal{P}(c)} \left(-p_c l_{pc} \mathbf{n}_{pc} + \mathbf{M}_{pc} (\mathbf{u}_p - \mathbf{u}_c) \right) \cdot \left(\mathbf{u}_p - \frac{\mathbf{u}_c^{n+1} + \mathbf{u}_c^n}{2} \right) \\
&= \sum_{p \in \mathcal{P}(c)} \mathbf{f}_{pc}^n \cdot \left(\mathbf{u}_p - \frac{\mathbf{u}_c^{n+1} + \mathbf{u}_c^n}{2} \right),
\end{aligned}$$

where the total internal energy e is defined by

$$me = \sum_k m^k e^k.$$

This discrete internal energy evolution equation may be combined with the kinetic energy equation (17) to recover the following discrete total energy equation

$$\frac{m_c}{\Delta t} \left(e_c^{n+1} - e_c^n + \left\| \mathbf{u}_c^{n+1} \right\|^2 / 2 - \left\| \mathbf{u}_c^n \right\|^2 / 2 \right) = \sum_{p \in \mathcal{P}(c)} \mathbf{f}_{pc}^n \cdot \mathbf{u}_p.$$

As in the monomaterial case, node velocities $\mathbf{u}_p$ are computed to ensure both discrete momentum and total energy conservation which concludes the proof. □

Property 2. *Temperature positiveness (ideal gas law)*
The positiveness of the discrete temperature may be ensured under CFL condition.

Proof. From the energy equation in (16) we show that the positiveness of the species numerical internal energy (and hence that of the temperature for ideal gas law) is ensured under the following CFL condition

$$\Delta t \leq \min_k \left\| \frac{m_c^k e_c^{k,n}}{K_c^k} \right\|_\infty,$$

where

$$\begin{aligned}
K_c^k =& \beta_c^k p_c \sum_{p \in \mathcal{P}(c)} l_{pc} \mathbf{n}_{pc} \cdot \mathbf{u}_p - \sum_{p \in \mathcal{P}(c)} (\mathbf{u}_p - \mathbf{u}_c)^T \mathbf{M}_{pc}^k (\mathbf{u}_p - \mathbf{u}_c) \\
&- p_c \left(\sum_i \frac{\alpha_c^i}{\rho_c^i (c_c^i)^2} \right) \left(\sum_i \beta_c^i \beta_c^k \Delta_c^{i,k} \right).
\end{aligned}$$

□

Property 3. *Semi-discrete entropy dissipation*
The semi-discrete entropy in each cell is dissipated per species:

$$m_c^k \frac{\mathrm{d}}{\mathrm{d}t}(\eta_c^k) \geq 0,$$

Proof. The semi-discrete entropy is written thanks to Gibbs' equation:

$$m_c^k T_c^k \frac{\mathrm{d}}{\mathrm{d}t}(\eta_c^k) = m_c^k \frac{d}{dt}(e_c^k) + m_c^k p_c^k \frac{d}{dt}\left(\frac{1}{\rho_c^k}\right).$$

Our discretization of the energy equation uses the mass equation one so that

$$m_c^k \frac{\mathrm{d}}{\mathrm{d}t}(e_c^k) = -m_c^k p_c^k \frac{\mathrm{d}}{\mathrm{d}t}\left(\frac{1}{\rho_c^k}\right) + \sum_{p\in\mathcal{P}(c)} (\mathbf{u}_p - \mathbf{u}_c)^T \mathbf{M}_{pc}^k (\mathbf{u}_p - \mathbf{u}_c).$$

Finally

$$m_c^k T_c^k \frac{\mathrm{d}}{\mathrm{d}t}(\eta_c^k) = \sum_{p\in\mathcal{P}(c)} (\mathbf{u}_p - \mathbf{u}_c)^T \mathbf{M}_{pc}^k (\mathbf{u}_p - \mathbf{u}_c) \geq 0.$$

Notice that the proof does not rely on the discretization of the mass equation. We only need both mass and energy equations to be coherent with each other. As a result, the semi-discrete entropy dissipation does not depend on the closure chosen for $\frac{\mathrm{d}}{\mathrm{d}t}(\rho^k)$; in particular, it is identical for the equal strain and the isopressure closures. □

3.6 Pressure relaxation procedure

Here it should be highlighted that the numerical strategy presented in the previous sections only enforces the pressure equality between materials in a mixed cell up to the scheme order. Consequently, as iterations accumulate, pressures may diverge from one another. This decoupling is clearly illustrated in the numerical section and decreasing the CFL number helps recovering a better pressure coupling. In order to keep a large CFL number, a relaxation procedure in the spirit of the ideas introduced in [9], is now presented. In practice, this correction is applied after the Lagrangian phase and remains particularly inexpensive since one starts with a pressure decoupling of order $\mathcal{O}(\Delta t)$. Of course, this process should be carefully done in order to preserve at the discrete level all the properties proven above. We now introduce the following notation

$$[X] = X^{\text{final}} - X^{\text{initial}},$$

where X is a physical quantity and the notation [.] represents the difference between a final state and an initial one. Our requirements for the relaxation procedure are as follows. Firstly, the procedure must be iso-volume (the global cell size must not be changed)

$$c_1[v_1] + c_2[v_2] = 0, \tag{18}$$

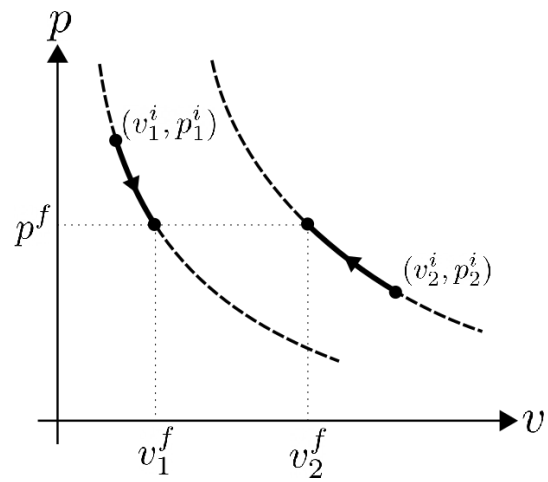

Figure 2: Visualization of the transformations in the (p, v) plane.

as well as iso-energy meaning that the total internal energy in the cell must be preserved

$$c_1[e_1] + c_2[e_2] = 0. \tag{19}$$

In addition, the process must be consistent with thermodynamics; therefore no entropy reduction should occur on any material involved. Considering thermodynamic paths $p_1(v_1)$ and $p_2(v_2)$ (see figure 2), we have

$$[e_k] = -\int_{v_k^i}^{v_k^f} p_k(v) dv_k + Q_k, \quad k \in \{1, 2\},$$

where Q_k corresponds to the entropy dissipation of material k. Defining the average pressure $< p_k >$ along the path, we then have

$$[e_k] = - < p_k > [v_k] + Q_k, \quad k \in \{1, 2\}.$$

Using both iso-volume and iso-energy assumptions, we eventually get

$$[e_k] = -(\beta_1 < p_1 > + \beta_2 < p_2 >)[v_k] = - < p > [v_k] \quad k \in \{1, 2\},$$

with

$$\beta_1 = \frac{c_2 Q_2}{c_1 Q_1 + c_2 Q_2}, \quad \beta_2 = \frac{c_1 Q_1}{c_1 Q_1 + c_2 Q_2}, \quad \beta_1 + \beta_2 = 1.$$

Because $< p >$ does not depend on the material, taking $p = p^f$ is a sensible choice. We now need to check whether or not the variation in entropy is positive. To do so, we apply the Taylor–Lagrange theorem to the entropy $\eta(v, e)$ (the indexes k are omitted for readability purposes) around the state (v^f, e^f). Then,

there is a convex combination $(\overline{v}, \overline{e})$ of the initial and final states for which

$$\eta^i = \eta^f + \left(\frac{\partial \eta}{\partial v}\right)^f (v^i - v^f) + \left(\frac{\partial \eta}{\partial e}\right)^f (e^i - e^f) + \frac{1}{2}\left(\nabla^2 \eta(\overline{v}, \overline{e})\right)(v^i - v^f, e^i - e^f),$$
$$= \eta^f + \frac{p^f}{T^f}(v^i - v^f) + \frac{1}{T^f}(e^i - e^f) + \frac{1}{2}\left(\nabla^2 \eta(\overline{v}, \overline{e})\right)(v^i - v^f, e^i - e^f).$$

Using both the equation $[e] = -p^f[v]$ and the concavity of the entropy, we finally get

$$[\eta] = -\frac{1}{2}\left(\nabla^2 \eta(\overline{v}, \overline{e})\right)(v^i - v^f, e^i - e^f) > 0.$$

Remark: On a unrelated note regarding the relaxation procedure, one may find that applying the Taylor-Lagrange theorem around the state (v^i, e^i) shows that the formula $[e] = -p^i[v]$ leads to $[\eta] < 0$.

To summarize, the following set of equations with unknowns v_1^f, v_2^f, e_1^f, e_2^f and p^f is solved with a standard Newton-Raphson method to enforce the isobar assumption

$$\begin{cases} c_1[v_1] + c_2[v_2] = 0, \\ p_1^f = p_2^f = p^f, \\ [e_1] = -p^f[v_1], \\ [e_2] = -p^f[v_2]. \end{cases}$$

Of course, the methodology naturally extends to an arbitrary number of materials.

4 Numerical test cases

Our scheme is now confronted with 1D and 2D test cases. Apart from the last one, where mesh entanglement imposes using a remap and relaxation procedure, all test cases are purely Lagrangian. The robustness and accuracy of our scheme is assessed, and the results are compared with that of a scheme based on the equal strain assumption.

4.1 Bi-fluid Piston

The system under consideration is that of a homogeneous mix of two perfect gases inside a piston, with same initial pressures, one having a very low volume fraction. The left border of the domain moves at velocity $\mathbf{u}_L$ which creates a shock. If the two gases have different equations of state, their compression rate needs to be different in order to maintain pressure equilibrium after the shock. Numerical results on figure 4 confirm equal strain assumption leads to a decoupling of pressures while our scheme, based on the equal pressure assumption, does not, even without the relaxation procedure. Apart from the

pressure decoupling, densities and internal energies are significantly different. This is of utmost importance when considering chemical reactions which may or not be triggered depending on an energy threshold. Finally, while assuring the equality of pressures, the iso-pressure assumption provides more sensible energy and density values.

	γ	α	ρ	p
Gas 1	1.4	10^{-5}	1	1.144
Gas 2	5/3	$1-10^{-5}$	1	1.144

Figure 3: Initial states inside the piston.

4.2 Saurel-Abgrall shock tube

The scheme is tested on a shock tube [26] for which the left side is filled with water while the right side is only air. The left and right states are

$$\begin{pmatrix}\rho_L\\ u_L\\ p_L\end{pmatrix} = \begin{pmatrix}10^3\\ 0\\ 10^9\end{pmatrix} \quad \text{and} \quad \begin{pmatrix}\rho_R\\ u_R\\ p_R\end{pmatrix} = \begin{pmatrix}50\\ 0\\ 10^5\end{pmatrix}.$$

The mesh consists of only pure cells, except at the interface where both air and water are present inside a mixed cell. Water is modeled with a stiffened gas ($\gamma^w = \frac{5}{3}$ and $\pi^w = 10$, see [16] for more details) ; air is assumed to behave as a perfect gas with $\gamma^a = 1.4$. Because equations of state are particularly different, equal strain assumption leads to a strong decoupling in pressures inside the mixed cell (see Figure 5). As of our scheme with equal pressure assumption, pressures stay close to one another but not strictly equal as no pressure relaxation procedure is added. However, it may be seen on Figure 6 that decreasing the CFL makes pressures converge to the same value as expected.

4.3 2D Multimaterial Sedov

We now consider the 2D Sedov problem [25], and we replace the single perfect gas with a mix of two perfect gases ($\gamma^1 = 1.4$ and $\gamma^2 = 5/3$) with equal constant heat capacities $c_v = 1$. At the initial time, we use uniform densities $\rho^1(t=0) = \rho^2(t=0) = 1$, uniform volume fractions $\alpha^1(t=0) = 1 - \alpha^2(t=0) = 1 - 10^{-3}$ and a null velocity $\boldsymbol{u}(t=0) = \mathbf{0}$. A total energy deposit of $\varepsilon^1_{\text{or}} = 0.244816$ is set for fluid 1 inside the center cell (this value ensures that the wave front radius is 1 at $t = 1$) and energy of fluid 2 is chosen so that both fluids have equal temperatures. Inside other cells, temperatures are set to $T^1 = T^2 = 10^{-10}$.

The numerical domain used is a square $[0, 1.2]^2$ discretized with 50 cells on each direction. As the test case is a reduction of a cylindrical physical phenomenon in a 2D plane, we impose a symmetry boundary condition on the

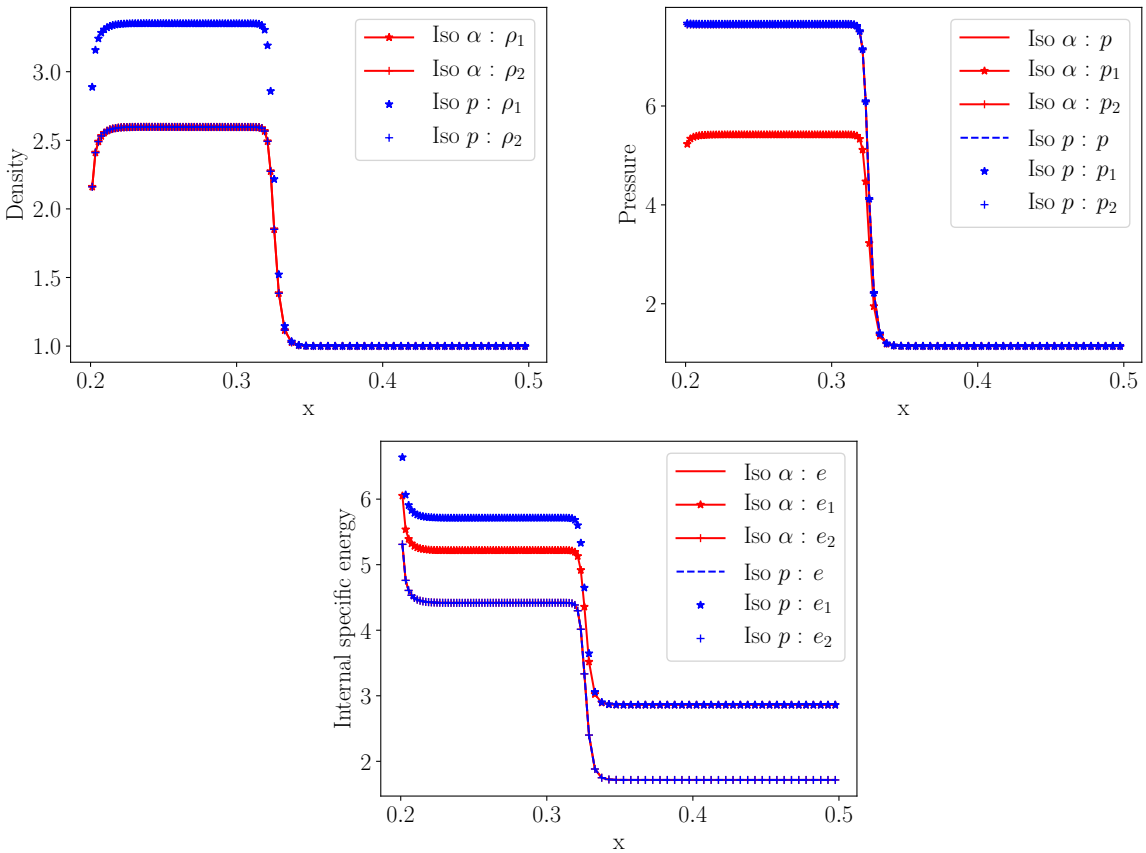

Figure 4: Comparison of equal pressure (Iso-p) scheme with equal strain assumption (Iso-α) scheme on a 100 cells mesh at final time $t = 0.2$.

left and on the bottom. On the right and on the top we impose a null velocity. The final time is 1.

Pressure difference is plotted on Figure 7 for both methods and different CFL values. Setting aside the central cell, the pressure decoupling is less intense for the equal pressure assumption based scheme. As for the central cell, the difference between pressures is still important, even bigger than that of the equal strain assumption scheme. This shows that if our scheme effectively deals with high contrasts of equations of state (see previous test case for example), it struggles with stiff initial conditions. This is because pressures are only kept equal up to scheme order. Hence, we believe that improving the order of the scheme would yield better results. In any case, Figure 7 shows that decreasing the CFL makes both pressures converge to the same limit (obviously not for the equal strain assumption).

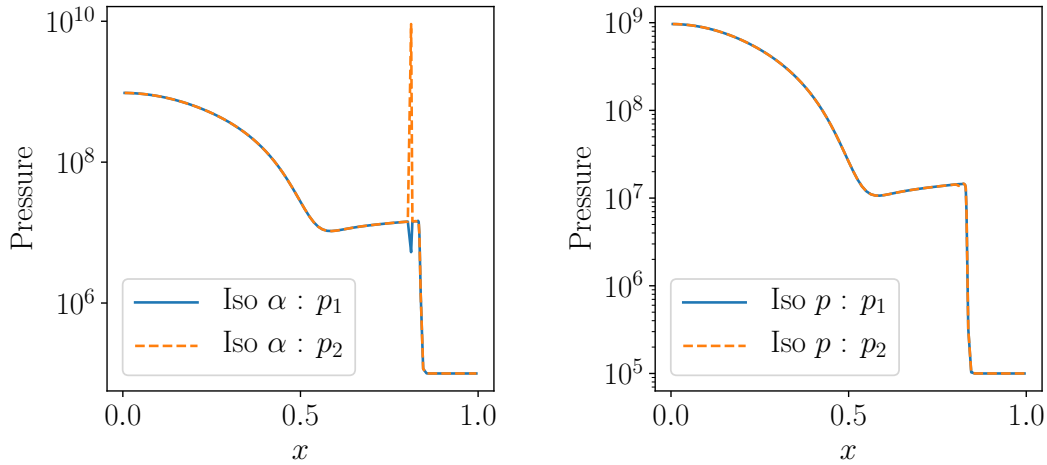

Figure 5: Saurel-Abgrall results a time $t = 2.2 \cdot 10^{-4}$ with 100 cells and a 0.99 CFL. Top: equal strain assumption (Iso-α); Bottom: equal pressure assumption (Iso-p).

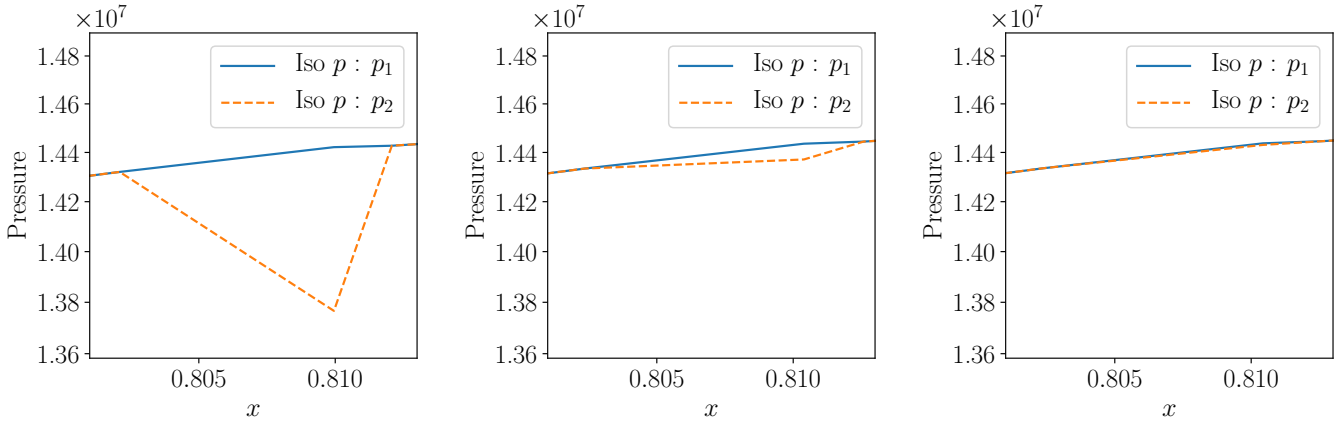

Figure 6: Zoom on the mixed cells for the Saurel-Abgrall shock tube a time $t = 2.2 \cdot 10^{-4}$ with 100 cells and different CFL. Left: CFL= 0.1; Right: CFL= 0.01.

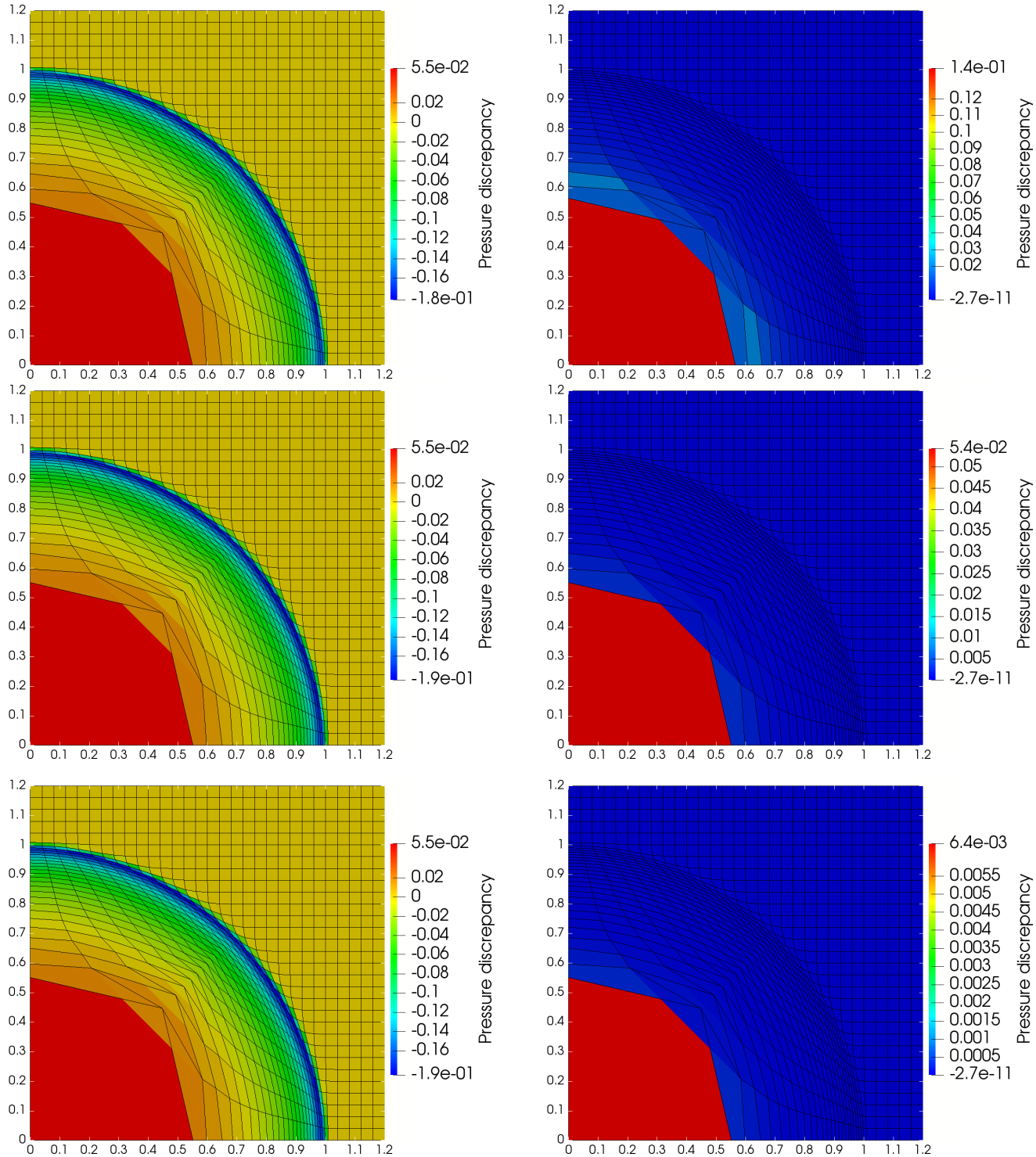

Figure 7: Pressure discrepancy for different CFL values. Left: equal strain assumption ; Right: equal pressure assumption. Top: CFL = 0.4 ; Middle: CFL = 0.04 ; Bottom: CFL = 0.004.

4.4 Shock through an air bubble

From [2], we consider an air bubble surrounded by water which is initially at equilibrium. A shock passes through the domain. Because air and water have highly different compressibility, the bubble is expected to collapse in on itself. A pure Lagrangian approach would not work here because of mesh entanglement. As a consequence, a remap procedure is added between the Lagrangian step and the pressure relaxation procedure.

The exact geometrical layout of the test case is now given, along with the physical quantities' value. The air bubble coincides with the disk of center $(0.5, 0.5)$ and radius 0.4 inside the domain $[-2, 2] \times [0, 1]$. Water is modeled with a stiffened gas ($\gamma^w = \frac{5}{3}$ and $\pi^w = 10$, see appendix for more details); air is assumed to behave as a perfect gas with $\gamma^a = 1.4$. Air is at pressure $p^a = 10^5$ and density $\rho^a = 1$. For $x > 0.04$, water is at pressure equilibrium with air $p_R^w = p^a = 10^5$ and has density $\rho_R^w = 10^3$. In order to initiate the shock, water pressure and density are set to $p_L^w = 3.10^9$ and $\rho_L^w = 1030.9$ inside the domain $x < 0.04$. A velocity gradient is also added with $u_L = (300, 0)$ when $x < 0.04$ and $u_R = (0, 0)$ when $x > 0.04$. Numerical results with a 600×300 mesh are displayed on Figure 8. Because of the high compressibility of air when mixed with water, the bubble shrinks until almost disappearing. Thanks to the pressure relaxation procedure, pressures are equal up to machine precision.

5 Conclusion

Following a discussion on volume fractions closure for a multimaterial model, a new cell-centered Lagrangian scheme has been presented in order to deal with the discretization of the equal pressure closure. The scheme derivation is motivated by thermodynamic considerations. A particular emphasis is put on entropy dissipation whose distribution over all material is an answer to the problem of multi-valued solutions when working with non-conservative equations. The scheme fares well when applied to test cases with high contrast of equations of state between materials. Perspectives are numerous. Improving the scheme order of accuracy could improve pressure equality without having to rely on low CFL numbers or pressure relaxation procedures. It would also reduce errors by helping capture more accurately solutions. Finally, an extension of this scheme to a multivelocity model is currently being investigated.

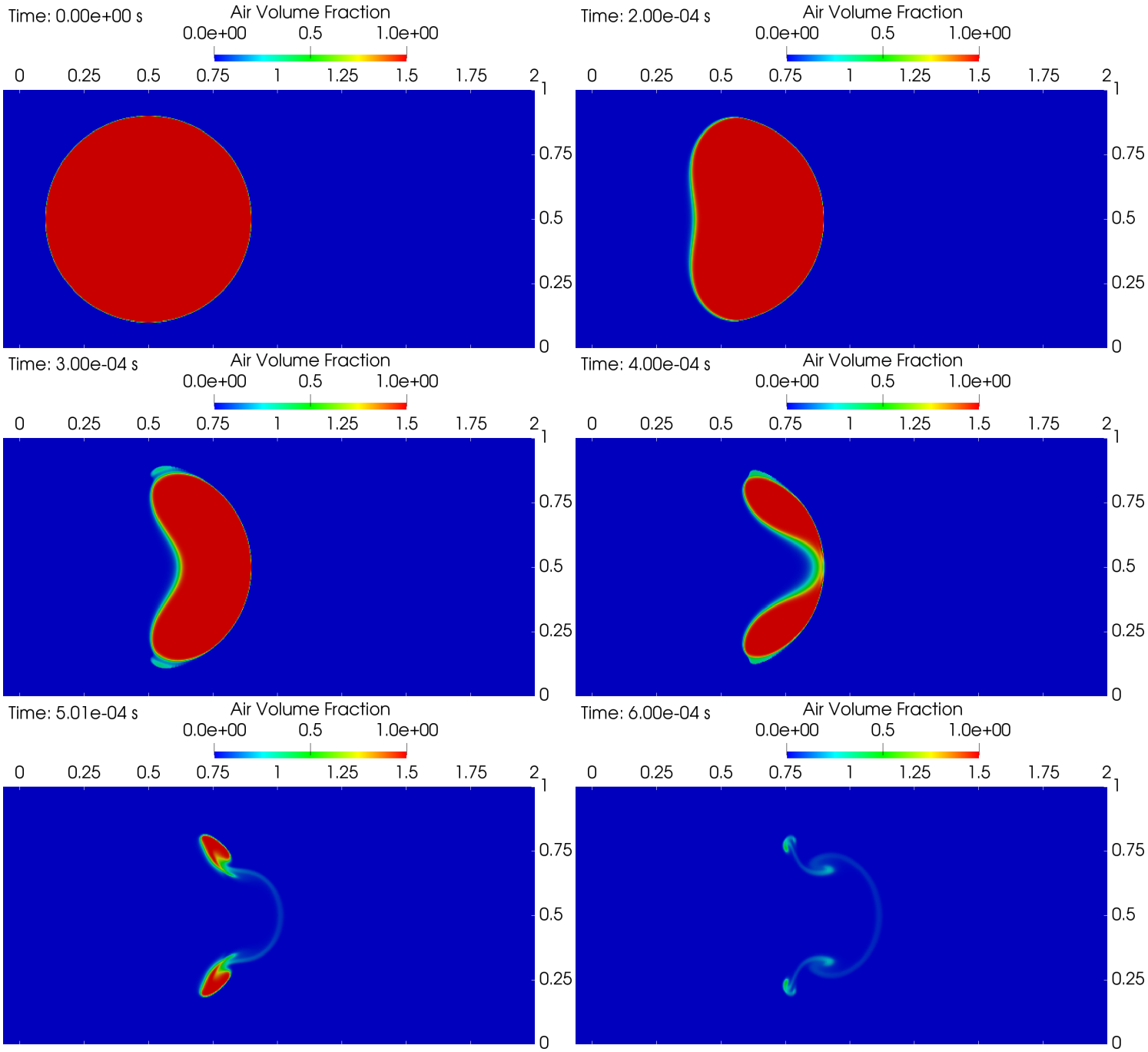

Figure 8: Air volume fraction for the air bubble test case at times $0, 3.10^{-4}, 2.10^{-4}, 4.10^{-4}, 5.10^{-4}$ and 6.10^{-4}.

A Hyperbolicity of the model

In this section, the hyperbolicity of the model is proven, in one dimension with an arbitrary number N of materials.

$$\begin{cases} \alpha^k \rho^k \dfrac{\mathrm{d}}{\mathrm{d}t}\left(\dfrac{1}{\alpha^k \rho^k}\right) - \partial_x u = 0, \\ \rho \dfrac{\mathrm{d}}{\mathrm{d}t}(u) + \partial_x p = 0, \quad p = \displaystyle\sum_k \alpha^k p^k, \\ \alpha^k \rho^k \dfrac{\mathrm{d}}{\mathrm{d}t}(e^k) + p^k \beta^k \partial_x u = 0, \\ \alpha^k \rho^k \dfrac{\mathrm{d}}{\mathrm{d}t}\left(\dfrac{1}{\rho^k}\right) - \beta^k \partial_x u = 0. \end{cases} \tag{20}$$

Assuming that, initially, pressures are the same for all materials, they remain equal at all times as

$$\begin{aligned} \frac{\mathrm{d}}{\mathrm{d}t}(p^k) &= (c^k)^2 \frac{\mathrm{d}}{\mathrm{d}t}(\rho^k) + \rho^k \Gamma^k T^k \frac{\mathrm{d}}{\mathrm{d}t}(s^k) \\ &= -(c^k)^2 (\rho^k)^2 \frac{\mathrm{d}}{\mathrm{d}t}\left(\frac{1}{\rho^k}\right) + \rho^k \Gamma^k \left[\frac{\mathrm{d}}{\mathrm{d}t}(e^k) + p^k \frac{\mathrm{d}}{\mathrm{d}t}\left(\frac{1}{\rho^k}\right)\right] \\ &= -\frac{1}{\sum_l \dfrac{\alpha^l}{(c^l)^2 \rho^l}} \nabla u, \end{aligned}$$

which does not depend on material k. Consequently, p may be replaced with any p^k depending on what suits us better in our computations. The model may be rewritten with variables $\mathbf{U} = (v^k = 1/(\alpha^k \rho^k), u, \tau^k = 1/\rho^k, s^k)$; for the sake of readability, it is only written for two materials:

$$\frac{\mathrm{d}}{\mathrm{d}t}(\mathbf{U}) + A(\mathbf{U}) \nabla \mathbf{U} = 0,$$

$$A(\mathbf{U}) = \begin{pmatrix} 0 & 0 & -v^1 & 0 & 0 & 0 & 0 \\ 0 & 0 & -v^2 & 0 & 0 & 0 & 0 \\ 0 & 0 & 0 & \tau \partial_{\tau^1} p^1 & \tau \partial_{\tau^2} p^2 & \tau \partial_{s^1} p^1 & \tau \partial_{s^2} p^2 \\ 0 & 0 & -\beta^1 v^1 & 0 & 0 & 0 & 0 \\ 0 & 0 & -\beta^2 v^2 & 0 & 0 & 0 & 0 \\ 0 & 0 & 0 & 0 & 0 & 0 & 0 \\ 0 & 0 & 0 & 0 & 0 & 0 & 0 \end{pmatrix}.$$

In order to find the eigenvalues and eigenvectors of $A(\mathbf{U})$, we first compute its characteristic polynomial. Immediately factoring the kth first columns of the determinant and then performing a Laplace expansion of the first column of the

resulting minor eventually leads to

$$\begin{aligned}\chi_A(X) &= X^{3N-1}\left[X^2 + \sum_k (\beta^k v^k \tau \partial_{\tau^k} p^k)\right] \\ &= X^{3N-1}\left[X^2 - \sum_k \left(\frac{\beta^k}{(\alpha^k)^2}(c^k)^2\right)\right].\end{aligned}$$

If all speeds of sound c^k are real, then the polynomial has only real roots. The two non-zero roots are of multiplicity one so the associated eigenspaces are necessarily of dimension one. However, zero is a root of multiplicity $3N-1$ so we need to check if the eigenspace is also of dimension $3N-1$ which is both sufficient and necessary for the matrix A to be diagonalizable. It may be quickly checked that equation $Ax = 0$ (with $x = (x_{v^k}, x_u, x_{\tau^k}, x_{s^k})$) is equivalent to system

$$\begin{cases} x_u = 0, \\ \sum_k (\partial_{\tau^k} p^k) x_{\tau^k} + \sum_k (\partial_{s^k} p^k) x_{s^k} = 0, \end{cases}$$

which consists in two independent equations. As a consequence, the eigenspace associated to the eigenvalue 0 is of dimension $(3N+1) - 2 = 3N - 1$ which shows that the matrix $A(\mathbf{U})$ is diagonalizable with real eigenvalues. Then, by definition, the system is hyperbolic.

References

[1] J.P. Boris and E.S. Oran. The numerical simulation of compressible reactive flows. *AIAA Papers No., 87-1323*, 1987.

[2] Jérôme Breil. *Numerical methods for Lagrangian and Arbitrary-Lagrangian-Eulerian Hydrodynamic Contribution to the simulation of High-Energy-Density-Physics Problems.* Habilitation à diriger des recherches, Univresité de Bordeaux, June 2016.

[3] J.W. Cahn and J.E. Hiliard. Free energy of a nonuniform system. *J. Chem. Phys. 28, 258-267*, 1958.

[4] G. Carré, S. Del Pino, B. Després, and E. Labourasse. A cell-centered lagrangian hydrodynamics scheme on general unstructured meshes in arbitrary dimension. *Journal of Computational Physics*, 228(14):5160–5183, 2009.

[5] C. Chalons. Path-conservative in-cell discontinuous reconstruction schemes for non conser- vative hyperbolic systems. *al-02263335*, 2019.

[6] R. Chauvin, S. Guisset, B. Manach-Perennou, and L. Martaud. A colocalized scheme for three-temperature grey diffusion radiation hydrodynamics. *Communications in Computational Physics*, 2021.

[7] Juan Cheng, Chi-Wang Shu, and Qinghong Zeng. A conservative lagrangian scheme for solving compressible fluid flows with multiple internal energy equations. *Communications in Computational Physics*, 12(5):1307–1328, 2012.

[8] E. Heulard de Montigny and A. Llor. Taming "stiff stiffness" of pressure work and equilibration in numerical schemes for compressible multi-fluid flows. *accepted to IJMF*, 2022.

[9] B. Després and F. Lagoutière. Numerical resolution of a two-component compressible fluid model with interfaces. *Progress in Computational Fluid Dynamics*, 2007.

[10] R.P. Fedkiw, T. Aslam, B. Merriman, and S. Osher. A non-oscillatory eulerian approach to interfaces in multimaterial flows (the ghost fluid method). *J. COmput. Phys. 152, 457-492*, 1999.

[11] J. GLimm, J.W. Grove, X.L. Li, K.M. Shyue, and Q. Zhang. Three-dimensional front tracking. *J. Sci. Comput, 19, 703-727*, 1998.

[12] Eric Heulhard de Montigny. *Thermo-hydro-dynamic consistency and stiffness in general compressible multiphase flows*. PhD thesis, 2021. Thèse de doctorat dirigée par Llor, Antoine Mathématiques aux interfaces université Paris-Saclay 2021.

[13] C. Hirt and B. Nichols. Volume of fluid (vof) method for the dynamics of free boundaries. *J. Comput. Phys.*, 39, 201 (1981).

[14] M. Ishii. *Thermo-fluid Dynamic Theory of Two-phase Flow*. Collection de la Direction des études et recherches d'Electricité de France. Eyrolles, 1975.

[15] Ashwani Kapila, R. Menikoff, J. Bdzil, Steven Son, and D. Stewart. Two-phase modeling of deflagration-to-detonation transition in granular materials: Reduced equations. *Phys. Fluids*, 13:3002–3024, 10 2001.

[16] Olivier Le Métayer and Richard Saurel. The noble-abel stiffened-gas equation of state. *Physics of Fluids*, 28(4):046102, 2016.

[17] Antoine Llor. Modèles hydrodynamiques statistiques pour les écoulements d'instabilités de mélange en régime développé: critères théoriques d'évaluation 0d et comparaison des approches mono et bifluides, 2001.

[18] P.H. Maire. Contribution to the numerical modeling of inertial confinement fusion. *Habilitation à Diriger des Recherches*, 2011.

[19] V. Maltsev, M. Skote, and P. Tsoutsanis. High-order methods for diffuse-interface models in compressible multi-medium flows: A review. *Physics of Fluids*, 34(2):021301, 2022.

[20] Gianni Dal Maso, Patrick Le Floch, and François Murat. Definition and weak stability of nonconservative products. *Journal de Mathématiques Pures et Appliquées*, 74:483–548, 1995.

[21] B.D. Nichols and C.W. Hirt. Improved free surface boundary conditions for numerical incompressible-flow calculations. *J. Comput. Phys. 8, 434-448*, 1971.

[22] B.J. Parker and D.L. Youngs. Two and three dimensional eulerian simulations of fluid flow with material interfaces. *Technical Report 01/92*, 1992.

[23] Christina Paulin. *Improved numerical schemes for monotonic conservative scalar advection : tackling mesh imprinting and numerical wetting.* PhD thesis, 2021. Thèse de doctorat dirigée par Llor, Antoine Mathématiques appliquées université Paris-Saclay 2021.

[24] J. Breil P.H. Maire, R. Abgrall and J. Ovadia. A cell-centered lagrangian scheme for two-dimensional compressible flow problems. *SIAM J.on Scientific Computing, Vol.29, No.4, p.1781-1824*, 2007.

[25] F.X. Timmes R. Kamm. On efficient generation of numerically robust sedov solutions. *LANL Report LA-UR-07-2849*, 2007.

[26] R. Saurel and R. Abgrall. A multiphase godunov method for compressible multifluid and multiphase flows. *Journal of Computational Physics*, 1999.

[27] Richard Saurel and Carlos Pantano. Diffuse-Interface Capturing Methods for Compressible Two-Phase Flows. *Annual Review of Fluid Mechanics*, 50(1):105 – 130, January 2018.

[28] M. Sussman. A level-set approach for computing solution to incompressible two-phase flow. *J Comput. Phys. 114, 146-159*, 1994.

[29] S.O. Unverdi and G. Tryggvason. A front-tracking method for viscous incompressible, multi-fluid flows. *J. Comput. Phys. 100, 25-37*, 1992.

[30] Thibaud Vazquez gonzalez. *Schémas numériques mimétiques et conservatifs pour la simulation d'écoulements multiphasiques compressibles.* PhD thesis, 2016. Thèse de doctorat dirigée par Llor, Antoine Mathématiques appliquées Université Paris-Saclay (ComUE) 2016.

[31] Thibaud Vazquez-Gonzalez, Antoine Llor, and Christophe Fochesato. A mimetic numerical scheme for multi-fluid flows with thermodynamic and geometric compatibility on an arbitrarily moving grid. *International Journal of Multiphase Flow*, 132:103324, 2020.

[32] Martin Wörner. *A compact introduction to the numerical modeling of multiphase flows*, volume 6932. FZKA, 2003.